

# **A Numerical Study of the Development of Frontal Motions**

**By  
Desiraju B. Rao  
and  
J. Michael Fritsch**

Contract No. F19628-68-C-0104

Project No. 8628  
Task No. 862804  
Work Unit No. 86280401

Scientific Report No. 4  
January 1971

Contract Monitor: Louis Berkofsky  
Meteorology Laboratory

This document has been approved for public release and sale; its distribution is unlimited.

Prepared for

Air Force Cambridge Research Laboratories  
Air Force Systems Command  
United State Air Force  
Bedford, Massachusetts 01730

Department of Atmospheric Science  
Colorado State University  
Fort Collins, Colorado

AFCRL-71-0320

**Colorado  
State  
University**

**Department of  
Atmospheric Science**

Paper No. 171

Qualified requestors may obtain additional copies from the Defense Documentation Center. All others should apply to the National Technical Information Service.

A NUMERICAL STUDY OF THE DEVELOPMENT  
OF FRONTAL MOTIONS

by

Desiraju B. Rao

and

J. Michael Fritsch

Department of Atmospheric Science  
Colorado State University  
Fort Collins, Colorado 80521

CONTRACT No. F19628-68-C-104  
Project No. 8628  
Task No. 862804  
Work Unit No. 86280401

SCIENTIFIC REPORT NO. 4

JANUARY 1971

Contract Monitor: Louis Berkofsky  
Meteorology Laboratory

This document has been approved for public  
release and sale; its distribution is unlimited.

Prepared for

AIR FORCE CAMBRIDGE RESEARCH LABORATORIES

AIR FORCE SYSTEMS COMMAND

UNITED STATES AIR FORCE

BEDFORD, MASSACHUSETTS 01730

Qualified requestors may obtain additional copies from the Defense Documentation Center. All others should apply to the National Technical Information Service.

\*

## ABSTRACT

\*

Development of frontal disturbances is considered from a non-linear initial value point of view. The frontal model is a two layer model with a wedge of cold air to the north represented by a homogeneous fluid layer of density  $\rho_1$ , and an overlying warm air layer represented by another homogeneous fluid of density  $\rho_2 (< \rho_1)$ . The warm and cold air layers have finite depths and the region of integration is bounded in the north-south direction by rigid boundaries. Inside this region, the depth of cold air goes to zero at some point, depicting the intersection of the frontal surface with the ground. The point of intersection essentially represents a free boundary. The west-east boundaries are periodic. A sinusoidal disturbance is imposed on the frontal surface and the growth of this disturbance is calculated numerically for two-different initial conditions. For each set of initial conditions, various wave lengths and initial shears are considered. The frontal surface at each time step is determined by a simple linear extrapolation of the cold air height fields from the north.

## I. INTRODUCTION

One of the characteristic features of the atmospheric motions in middle latitudes is the motion of wave like disturbances which propagate on a surface of discontinuity between a layer of cold air near the ground and an overlying layer of warm air. The theory associated with the development of these disturbances was originally formulated by the Bergen School of Norway and is now referred to as the polar front theory (Bjerknes and Solberg 1922). The layer of cold air occupies a wedge shaped area to the north with the depth of the cold air being zero at some point and increasing north of that point as shown in Figure 1. The warm air is superimposed on this cold air layer. The transition from the cold air mass to the warm air mass occurs through a narrow zone which is normally characterized by strong temperature and wind gradients. This finite transition zone is idealized as a surface of discontinuity and it is found that wave like disturbances on this frontal surface grow in time to generate frontal cyclones.

For theoretical purposes, the warm and cold air layers are represented by incompressible, homogeneous fluids of different densities on a plane of constant rotation. Each of the fluid layers moves with some constant zonal speed so that there is a discontinuity in the tangential speed at the frontal surface. The existence of non-zero zonal velocities in the basic state on a rotating plane then produces a slope of the frontal surface in the north-south direction to balance the coriolis forces acting on the zonal wind. The theoretical studies on such an idealized frontal configuration were first approached using a perturbation method or stability considerations.

One of the earliest theoretical attempts at the stability analysis was that of Solberg (1928) [see also Bjerknes and Godske 1936]. Later, the stability studies on frontal models were considered by Kotschin (1932), Hlliasen (1960), and Orlanski (1968). The purpose of the stability studies is to determine whether waves of incipient cyclone scales can indeed become unstable in a linearized sense for the typically observed range of tangential velocity shear and the density ratio between the warm and cold air masses. However, the results from a linearized analysis can at best give an indication of the behavior of the perturbation initially. Once a perturbation starts growing, the non-linear effects will become important which would completely alter its subsequent behavior.

The importance of non-linear effects for the development of frontal disturbances was pointed out by Freeman (1952), Abdullah (1949) and Tepper (1952) who treated the frontal problem using the method of characteristics which restricts the treatment to only one space dimension. Kasahara et al (1965) solved the full two-dimensional non-linear shallow water equations for the motion of frontal disturbances assuming an infinitely deep upper layer. By this assumption, the dynamics of the warm air and its influence on the cold air are ignored and the number of dependent variables in the problem are reduced to three: the x and y-components of the velocity and the height of the cold air. The initial sinusoidal disturbance on the frontal surface is represented by marker particles and a quasi-Lagrangian approach is taken in keeping track of the future movement of these particles. The results obtained by Kasahara et al (ibid) showed a realistic distortion of the initial sinusoidal wave and a

tendency towards occlusion. The non-linear frontal problem was subsequently considered by Alterman and Isaacson (1969) using a two-layer model but with only one-space dimension. Eliassen and Raustein (1968) considered the frontal problem using isentropic co-ordinates. Grammelvedt (1970) considered the two-layer problem using material particles to calculate the frontal position by a method different from Kasahara et al (ibid).

In the present study, we considered the growth of a frontal disturbance using the two-dimensional quasi-static equations of a two-layer system. The dynamical equations are solved by finite-difference integrations for a few different initial conditions. In order to keep the computations relatively simple, the frontal surface, which is defined as the point where the cold air depth is zero, is determined, at each time step, by a linear extrapolation of the cold air depth field from the north. Admittedly, this method of locating the frontal surface is not as accurate as the method used by Kasahara et al (ibid). Nevertheless, the results obtained by using the simple extrapolation technique on a one-layer model identical to that of Kasahara et al (ibid) have shown that the differences in the frontal motion are not too significant.

## 2. DYNAMICAL EQUATIONS

We consider two incompressible homogeneous fluids of densities  $\rho_1$  and  $\rho_2$ , super-imposed one on top of another in a gravitationally stable configuration as shown in Figure 1. The heavier fluid ( $\rho_1$ ) represents the cold air and the lighter fluid ( $\rho_2$ ) the warm air. Each of these fluids is initially moving with a different but constant translational speed ( $\bar{u}_1$  and  $\bar{u}_2$ ) in the eastward direction. This fluid configuration is bounded by rigid boundaries to the north and south and rotating about a vertical axis with constant angular speed of rotation ( $\Omega$ ). In addition to the assumption of constant speed of rotation, we assume that the horizontal scale of the motions is much larger than the depth of the fluids so that the quasi-static (or shallow water) approximation may be made. This assumption is equivalent to assuming that the vertical accelerations are negligible and the pressure field is hydrostatically determined by the mass of the fluid above a point. A consequence of the quasi-static approximation is that if the horizontal velocity fields are initially independent of depth, they will remain independent of depth for all time. The pressure field in each layer then may be written as:

$$p_2 = g\rho_2(h-z) \quad h_1 \leq z \leq h \quad (1)$$

$$p_1 = g\rho_1(h_1-z) + g\rho_2(h-h_1) \quad 0 \leq z \leq h_1 .$$

In equation (1),  $h$  represents the total depth of the fluid,  $h_1$  the depth of the cold layer and  $g$  represents the gravitational force/unit mass.

The dynamic condition of pressure continuity at the interface  $z = h_1$  is automatically satisfied by equation (1). The dynamical equations may now be written as:

$$\frac{\partial \mathbf{V}_1}{\partial t} + \mathbf{V}_1 \cdot \nabla \mathbf{V}_1 - f[\mathbf{V}_1] = -g\nabla h_1 - g\epsilon \nabla (h - h_1). \quad (2)$$

$$\frac{\partial h_1}{\partial t} + \mathbf{V}_1 \cdot \nabla h_1 + h_1 \nabla \cdot \mathbf{V}_1 = 0 \quad (3)$$

$$\frac{\partial \mathbf{V}_2}{\partial t} + \mathbf{V}_2 \cdot \nabla \mathbf{V}_2 - f[\mathbf{V}_2] = -g\nabla h \quad (4)$$

$$\frac{\partial h_2}{\partial t} + \mathbf{V}_2 \cdot \nabla h_2 + h_2 \nabla \cdot \mathbf{V}_2 = 0 \quad (5)$$

In the above equations,  $f = 2\Omega \sin\theta$  is the coriolis parameter.  $\mathbf{V} = (u, v)$  is the horizontal velocity vector with the components  $u, v$  in the  $x, y$ -directions. The vector  $[\mathbf{V}]$  indicates a rotation of  $\mathbf{V}$  through ninety-degrees in the negative sense of the  $x, y$ -plane.  $\epsilon (\equiv \rho_2/\rho_1)$  is the density ratio of the two fluids and  $0 < \epsilon < 1$  for a gravitationally stable configuration.  $\nabla$  is the horizontal gradient operator.  $h_2 = h - h_1$  represents the depth of the warm air. The above equations have an exact solution corresponding to the state given by:

$$\mathbf{V}_1 = (\bar{u}_1, 0) ; \quad \mathbf{V}_2 = (\bar{u}_2, 0) \quad (6)$$

where  $u_1$  and  $u_2$  are constants or possibly some functions of  $y$ . Corresponding to equation (6) we obtain from equations (2-5):

$$\frac{\partial \bar{h}_1}{\partial x} = 0 = \frac{\partial \bar{h}_2}{\partial x}$$

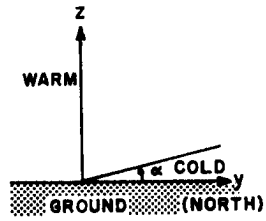


Figure 1  
Vertical cross section of the frontal model.

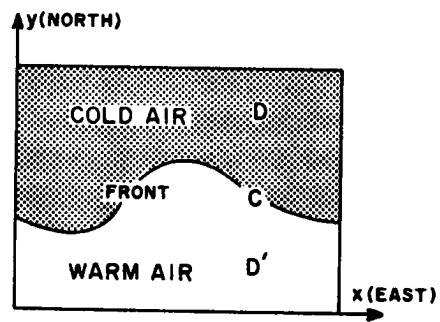


Figure 2  
The domain of integration.

$$\frac{\partial \bar{h}}{\partial x} = - \frac{f}{g} \frac{\epsilon \bar{u}_2 - \bar{u}_1}{1 - \epsilon} \quad (7)$$

$$\frac{\partial \bar{h}}{\partial y} = - \frac{f}{g} \bar{u}_2$$

The second of the above formulas is the Margule's formula for the slope of the frontal surface. Equations (7) show that both the interface and the free surface slope in the north-south direction in order to generate the necessary pressure gradients which balance the coriolis forces in the basic state.

We now have to solve the system of equations (2-5) subject to some initial and boundary conditions. As shown in Figure 2, the domain of integration consists of two regions D and D'. In domain D, we have cold air below and warm air above and in domain D' we have only warm air. The surface C separating the two domains is the frontal surface. The domains D and D' are bounded to the north and south respectively by rigid boundaries. The boundary conditions appropriate to this system are:

$$\begin{aligned} v_1 = 0, v_2 = 0 & \text{ at } y = y_N \\ v_2 = 0 & \text{ at } y = y_S \end{aligned} \quad (8)$$

which simply states that the normal velocity of the fluids vanishes on the rigid boundaries. In the west-east direction, we assume all quantities are periodic. If the length of the domain of integration in x-direction is L, then this condition states:

$$\alpha(x) = \alpha(x+L). \quad (9)$$

where  $\alpha$  is any one of the dependent variables. The frontal surface C is defined by the condition

$$h_1(x, y, t) = 0 \quad (10)$$

The warm air velocity and height fields are assumed to change continuously as we proceed from domain D to D' across the frontal surface.

The initial conditions here are the following:

Case (i): Only the zonal flow is assumed to be geostrophic. The initial conditions are

$$\begin{aligned} u_1 &= \bar{u}_1, \quad u_2 = \bar{u}_2 \\ v_1 &= 0, \quad v_2 = 0 \\ \bar{h}_1 &= \frac{f}{g} \frac{\epsilon \bar{u}_2 - \bar{u}_1}{1-\epsilon} (y-y_c) \text{ for } y_c \leq y \leq Y. \\ \bar{h}_1 &= 0 \text{ for } 0 \leq y \leq y_c \\ \bar{h}_2 &\equiv \bar{h} - \bar{h}_1 = H_0 - \frac{f \bar{u}_2}{g} y \text{ for } 0 \leq y \leq y_c \\ &= H_0 - \frac{f}{g} \left[ \frac{\bar{u}_2 (y - \epsilon y_c) - \bar{u}_1 (y - y_c)}{1-\epsilon} \right] \text{ for } y_c \leq y \leq Y. \end{aligned} \quad (11)$$

In the above equations, Y is the north-south width of the channel.

$y_c$  represents the initial disturbance superimposed on the frontal surface and is given by

$$y_c = a \sin(kx + \delta) + b$$

where a, b, and  $\delta$  are constants.  $H_0$  in equation (11) represents the depth of the warm air at the southern boundary. The equation for  $y_c$

determines the  $y$  co-ordinate of the front as a function of  $x$ . One can represent  $y_c$  by a certain number of particles and apply the equations of motion to these particles to calculate their trajectories. This is essentially the procedure adopted by Kasahara et al (ibid). Here, however, we have determined the  $y$  co-ordinate of the frontal surface, using the condition

$$h_1 = 0 \quad (12)$$

as a function of  $x$ , by simple linear extrapolation of the cold air depth field from the north.

Case (ii): Initially both the zonal as well as the meridional flows are assumed to be geostrophic. The height fields are given by the same formulas as in equation (11), but the zonal and meridional velocity fields are given by:

$$\begin{aligned} v_1 &= \frac{g}{f} \left[ \frac{\partial \bar{h}_1}{\partial x} + \epsilon \frac{\partial \bar{h}_2}{\partial x} \right], & v_2 &= \frac{g}{f} \frac{\partial \bar{h}}{\partial x} \\ u_1 &= -\frac{g}{f} \left[ \frac{\partial \bar{h}}{\partial y} + \epsilon \frac{\partial \bar{h}_1}{\partial y} \right], & \bar{u}_2 &= -\frac{g}{f} \frac{\partial \bar{h}}{\partial y} \end{aligned} \quad (13)$$

For computational purposes, it proves convenient to introduce the following non-dimensionalization scheme.

$$\begin{aligned} \zeta &\equiv \frac{x - \bar{u} \Delta t}{\Delta s}, \quad \eta \equiv \frac{y}{\Delta s}, \quad \tau \equiv \frac{t}{\Delta t}, \quad \bar{u} \equiv \frac{1}{2}(\bar{u}_1 + \bar{u}_2) \\ \hat{u}_i &\equiv (u_i - \bar{u}) \frac{\Delta t}{\Delta s} \\ \hat{v}_i &\equiv v_i \frac{\Delta t}{\Delta s} \end{aligned} \quad (14)$$

$$\hat{h}_i \equiv h_i g \left( \frac{\Delta t}{\Delta s} \right)^2$$

$$F \equiv f \Delta t$$

In the above equations,  $\Delta t$  and  $\Delta s$  are units of time and space. By introducing the non-dimensional quantities in equations (2, 3, 4, 5) and dropping the caps on  $u$ ,  $v$  and  $h$ , on the understanding that all quantities are now non-dimensional, we obtain

$$\frac{\partial \mathbb{V}_1}{\partial \tau} + \mathbb{V}_1 \cdot \nabla \mathbb{V}_1 - F[\mathbb{V}_1] = -\varepsilon \nabla(h-h_1) - \nabla h_1 - F \left( \frac{\bar{u} \Delta t}{\Delta s} \right) \mathbb{j}\mathbb{j} \quad (15)$$

$$\frac{\partial h_1}{\partial \tau} + \nabla \cdot (h_1 \mathbb{V}_1) = 0 \quad (16)$$

$$\frac{\partial \mathbb{V}_2}{\partial \tau} + \mathbb{V}_2 \cdot \nabla \mathbb{V}_2 - F[\mathbb{V}_2] = -\nabla h - F \left( \frac{\bar{u} \Delta t}{\Delta s} \right) \mathbb{j}\mathbb{j} \quad (17)$$

$$\frac{\partial h_2}{\partial \tau} + \nabla \cdot (h_2 \mathbb{V}_2) = 0 \quad (18)$$

In these equations  $\mathbb{j}\mathbb{j}$  is the unit vector in the  $y$ -direction. Gradient operator  $\nabla$  is given by  $\nabla \equiv \mathbb{i}\mathbb{i} \partial/\partial \zeta + \mathbb{j}\mathbb{j} \partial/\partial \eta$ .

### 3. FINITE-DIFFERENCE EQUATIONS

The domain of integration with sides of lengths  $L_1$  and  $L_2$  in the  $\zeta$  and  $\eta$  directions is divided into rectangular mesh such that the coordinates are given by  $\zeta_j = j\Delta\zeta$ ,  $\eta_i = i\Delta\eta$  where  $\Delta\zeta$ ,  $\Delta\eta$  are the grid intervals in the  $\zeta$  and  $\eta$  directions. The continuous equations (15 and 17) are written in an advective form:

$$\frac{\partial \mathbf{V}_1}{\partial \tau} + \nabla \cdot \mathbf{V}_1 \mathbf{V}_1 - \mathbf{V}_1 \nabla \cdot \mathbf{V}_1 - F[\mathbf{V}_1] = -\varepsilon \nabla(h-h_1) - \nabla h_1 - F\left(\frac{\bar{u}\Delta t}{\Delta s}\right)_{jj} \quad (19)$$

$$\frac{\partial \mathbf{V}_2}{\partial \tau} + \nabla \cdot \mathbf{V}_2 \mathbf{V}_2 - \mathbf{V}_2 \nabla \cdot \mathbf{V}_2 - F[\mathbf{V}_2] = -\nabla h - F\left(\frac{\bar{u}\Delta t}{\Delta s}\right)_{jj} \quad (20)$$

Define now the following finite difference operators:

$$\alpha_x = \frac{1}{\Delta} \left\{ \alpha(x_i + \frac{\Delta}{2}) - \alpha(x_i - \frac{\Delta}{2}) \right\}$$

$$\bar{\alpha}^x = \frac{1}{2} \left\{ \alpha(x_i + \frac{\Delta}{2}) + \alpha(x_i - \frac{\Delta}{2}) \right\}$$

where  $\alpha$  is any variable and  $\Delta (= \Delta\zeta \text{ or } \Delta\eta)$  is the grid interval. Then, using the definitions, we get

$$\frac{\partial \alpha}{\partial \zeta} = \alpha_{\zeta}^{\zeta},$$

$$\frac{\partial \alpha}{\partial \eta} = \alpha_{\eta}^{\eta}$$

Let us define in addition:

$$\left( \alpha_{\zeta}^{\zeta} \beta_{\zeta}^{\zeta} \right)_{\zeta} = \alpha_{\zeta\zeta}^{\zeta\zeta} \beta_{\zeta}^{\zeta} + \beta_{\zeta\zeta}^{\zeta\zeta} \alpha_{\zeta}^{\zeta}.$$

Table 1. Initial Conditions

	A	B
$u_1$ zonal velocity of cold air (m/sec)	3.05	10
$v_1$ meridional velocity of cold air (m/sec)	0	see eq (13)
$u_2$ zonal velocity of warm air (m/sec)	15.53	20
$v_2$ meridional velocity of warm air (m/sec)	0	0
$\bar{u}$ velocity of coordinate system (m/sec)	3.05	15
north and south boundary condition	$v = 0$	$v = 0$
$f$ Coriolis parameter ( $\text{sec}^{-1}$ )	$10^{-4}$	$10^{-4}$
$\epsilon$ density discontinuity (non-dimensional)	0.9813386995	0.980
$h_2$ height of warm layer (km)	infinite	see eq (11)
$h_1$ height of cold layer (km)	see eq (11)	see eq (11)
$H_0$ height of warm layer at $\eta = 0$ (km)	infinite	15
$\Delta s$ grid length (km)	76.2	76.2
$L$ east-west extent of grid (km)	$20\Delta s$	$20\Delta s$
$a$ amplitude of initial wave	$2\Delta s$	$2\Delta s$
$b$ positional constant	$9.5\Delta s$	$21.37\Delta s$

where

$$\bar{\alpha}^{\zeta\zeta} = \frac{1}{4}[\alpha(x_i + \Delta) + 2\alpha(x_i) + \alpha(x_i - \Delta)].$$

Using these notations, the governing equations (16, 18, 19, 20) may be expressed as follows: These equations are written in component form now for convenience.

$$\begin{aligned} \frac{\partial u_1}{\partial \tau} = & - (\bar{u}_1^{\zeta} \bar{u}_1^{\zeta})_{\zeta} - (\bar{u}_1^{\eta} \bar{v}_1^{\eta})_{\eta} + u_1 (\bar{u}_1^{\zeta} + \bar{v}_1^{\eta}) \\ & + Fv_1 - \epsilon (\bar{h}_{\zeta}^{\zeta} - \bar{h}_1^{\zeta}) - \bar{h}_1^{\zeta} \end{aligned} \quad (21)$$

$$\begin{aligned} \frac{\partial v_1}{\partial \tau} = & - (\bar{u}_1^{\zeta} \bar{v}_1^{\zeta})_{\zeta} - (\bar{v}_1^{\eta} \bar{v}_1^{\eta})_{\eta} + v_1 (\bar{u}_1^{\zeta} + \bar{v}_1^{\eta}) - Fu_1 \\ & - (F \frac{\bar{u}\Delta t}{\Delta s}) - \epsilon (\bar{h}_{\eta}^{\eta} - \bar{h}_1^{\eta}) - \bar{h}_1^{\eta} \end{aligned} \quad (22)$$

$$\frac{\partial h_1}{\partial \tau} = - (\bar{h}_1^{\zeta} \bar{u}_1^{\zeta})_{\zeta} - (\bar{h}_1^{\eta} \bar{v}_1^{\eta})_{\eta} \quad (23)$$

for the lower layer. For the upper layer, we obtain

$$\begin{aligned} \frac{\partial u_2}{\partial \tau} = & - (\bar{u}_2^{\zeta} \bar{u}_2^{\zeta})_{\zeta} - (\bar{u}_2^{\eta} \bar{v}_2^{\eta})_{\eta} + u_2 (\bar{u}_2^{\zeta} + \bar{v}_2^{\eta}) \\ & + Fv_2 - \bar{h}_{\zeta}^{\zeta} \end{aligned} \quad (24)$$

$$\begin{aligned} \frac{\partial v_2}{\partial \tau} = & - (\bar{u}_2^{\zeta} \bar{v}_2^{\zeta})_{\zeta} - (\bar{v}_2^{\eta} \bar{v}_2^{\eta})_{\eta} + v_2 (\bar{u}_2^{\zeta} + \bar{v}_2^{\eta}) \\ & - Fu_2 - (F \frac{\bar{u}\Delta t}{\Delta s}) - \bar{h}_{\eta}^{\eta} \end{aligned} \quad (25)$$

$$\frac{\partial h_2}{\partial \tau} = - (\bar{h}_2^{\zeta} \bar{u}_2^{\zeta})_{\zeta} - (\bar{h}_2^{\eta} \bar{v}_2^{\eta})_{\eta} \quad (26)$$

The integration in time is performed using the Heun method which is a one-step method requiring information at only the preceding time level in order to proceed to the next time level (see Lilly 1965, Young 1968). Each of the preceding equations is in the form

$$\frac{\partial \alpha_i}{\partial \tau} = f(\alpha_1, \alpha_2, \dots, \alpha_6, t) \quad (27)$$

where the quantity on the right is known at any given instant. Then the time integration proceeds according to the formula:

$$\begin{aligned} \alpha^{(n+1)*} &= \alpha^{(n)} + f^{(n)} \Delta t \\ \alpha^{(n+1)} &= \alpha^{(n)} + \frac{1}{2}(f^{(n)} + f^{(n+1)*})\Delta t \end{aligned}$$

where the quantity  $f^*$  is evaluated using the value of  $\alpha^*$ .

#### 4. METHOD OF INTEGRATION

The integration is performed using the numerical constants given in Table 1. At each time step the integration starts from the northern boundary and proceeds southwards. At the northern boundary the meridional components of the velocity fields  $v_1$  and  $v_2$  are always zero, but we need to calculate the zonal components  $u_1$ ,  $u_2$  and the height fields  $h_1$  and  $h$ . In the equations (21, 23, 24, 26) governing this calculation, the quantity  $\partial v / \partial \eta$  on the boundary is required. This is obtained by fitting a quadratic curve to three points - the boundary point and the first two interior points - and differentiating this expression to determine  $\partial v / \partial \eta$  on the northern boundary. Similar situation occurs on the southern boundary in calculating the  $u_2$  and  $h$  fields and the same procedure is adopted there.

The integration then proceeds southward from the northern boundary until a grid point is reached where it is no longer possible to apply the central difference formula either in the  $\zeta$  or  $\eta$ -directions because of the fact that the domain  $D$  is getting terminated. For example, see points marked 1, 2, and 3, in Figure 3. In such cases, a rather simple extrapolation procedure was used using the two points immediately north of points, such as 1, 2, or 3, to first determine the  $\eta$ -co-ordinate corresponding to the frontal surface - namely, the  $h_1 = 0$  point. The values for  $u_1$ ,  $u_2$ ,  $v_1$ ,  $v_2$ ,  $h$ ,  $h_1$  are then calculated at points 1 and 2 using the formula generated by the two-point extrapolation. Attempts at using three points instead of two for the extrapolation purposes have proved rather unsuccessful since the  $\eta$ -co-ordinate corresponding to  $h_1 = 0$  has to be solved as the appropriate root of a quadratic equation and there

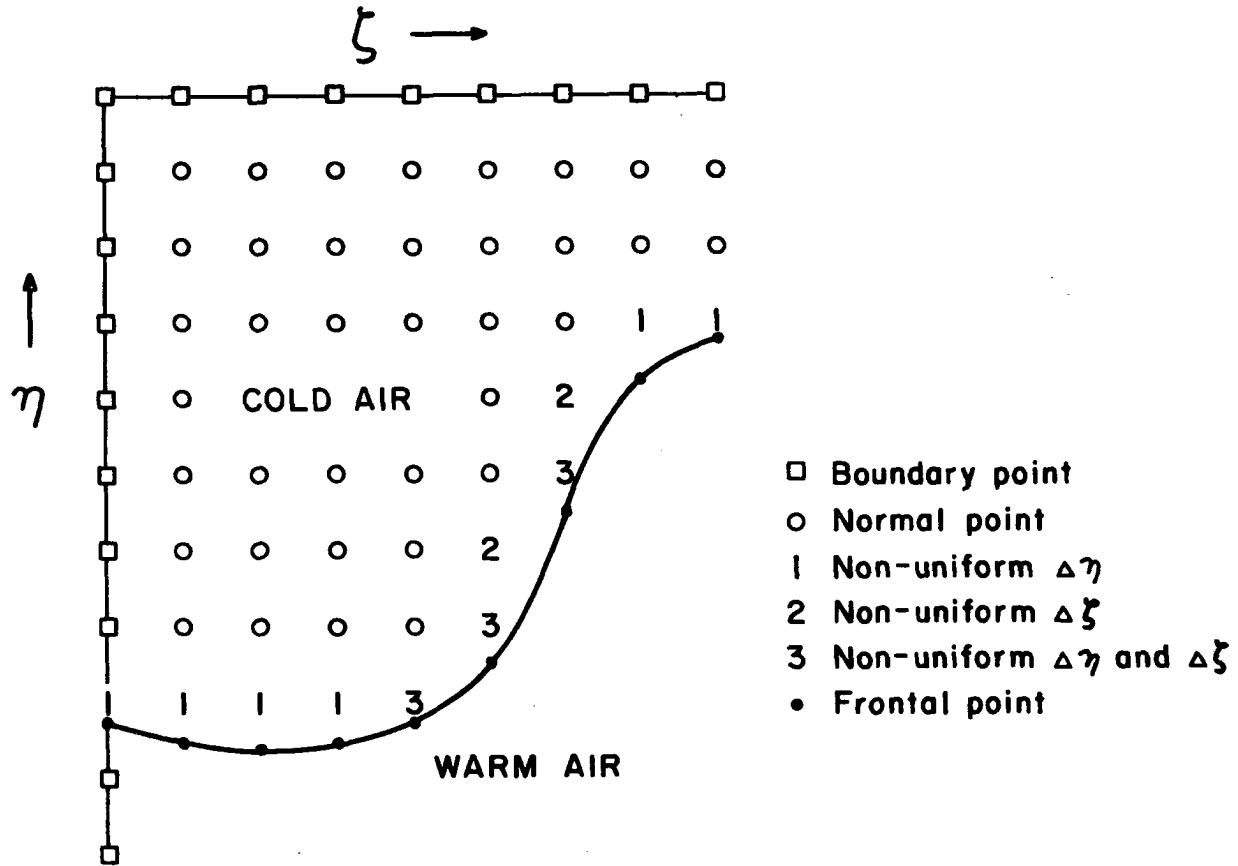


Figure 3  
Types of grid points.

is no obvious a priori argument to show which root of the quadratic is the right one. Further, the radical has occasionally become imaginary. In view of these difficulties, a simple linear extrapolation has been adopted. This is one of the serious limitations imposed by this study. However, a comparison of the results obtained by this method with the more rigorous technique of Kasahara et al on a one-layer model showed, as mentioned earlier, a good agreement in a qualitative sense. The frontal surface thus determined marks the end of domain D where the cold and warm air layers have existed together. The integration proceeds south now into the domain D' where only the warm air component exists using the fact that  $u_2$ ,  $v_2$ , and  $h_2$  are continuous across the frontal surface. The computations were smoothed every 30 time steps using the formula

$$\alpha_{i,j} = \frac{\alpha_{i+1,j} + \alpha_{i-1,j} + \alpha_{i,j+1} + \alpha_{i,j-1} + 4\alpha_{i,j}}{8} \quad (28)$$

in order to minimize the noise generated by the finite-difference integrations.

## 5. RESULTS

Various initial conditions representative of observed atmospheric conditions were selected for investigation. In addition, the frontal motion was determined for the same initial conditions (Table 1, column A) as used by Kasahara, Isaacson, and Stoker (ibid). Since in the latter model the dynamics of the warm layer have been neglected by assuming an infinitely deep warm layer, the numerical problem reduces to one of predicting only the motion of the cold air. This particular problem shall be referred to as the "one layer" case.

Even though the initial conditions and the governing equations of a physical system may be the same, the solution to the system may change slightly due to differences in numerical integration schemes. In the frontal problem, an additional discrepancy may occur since the method for calculating the frontal position is also variable (see section 4). Figure 4 shows the initial frontal position and the subsequent position after eight hours for the one layer model from Kasahara et al and from using the procedure described in section 4. As is evident from this diagram, except for the crest of the wave, the agreement in the results is fairly good. The curvature at the crest was reduced primarily by a Laplacian type smoothing operation which was used for controlling noise effects. This smoothing operation tended to flatten heights in areas where the slope of the height changed sign, for example, at the crest of the wave.

Since the real atmosphere frequently exhibits significant interaction between upper air dynamics and low level wave development, it was desirable to determine the effect of including the dynamics of a finite upper layer on the system described above. Therefore, for the

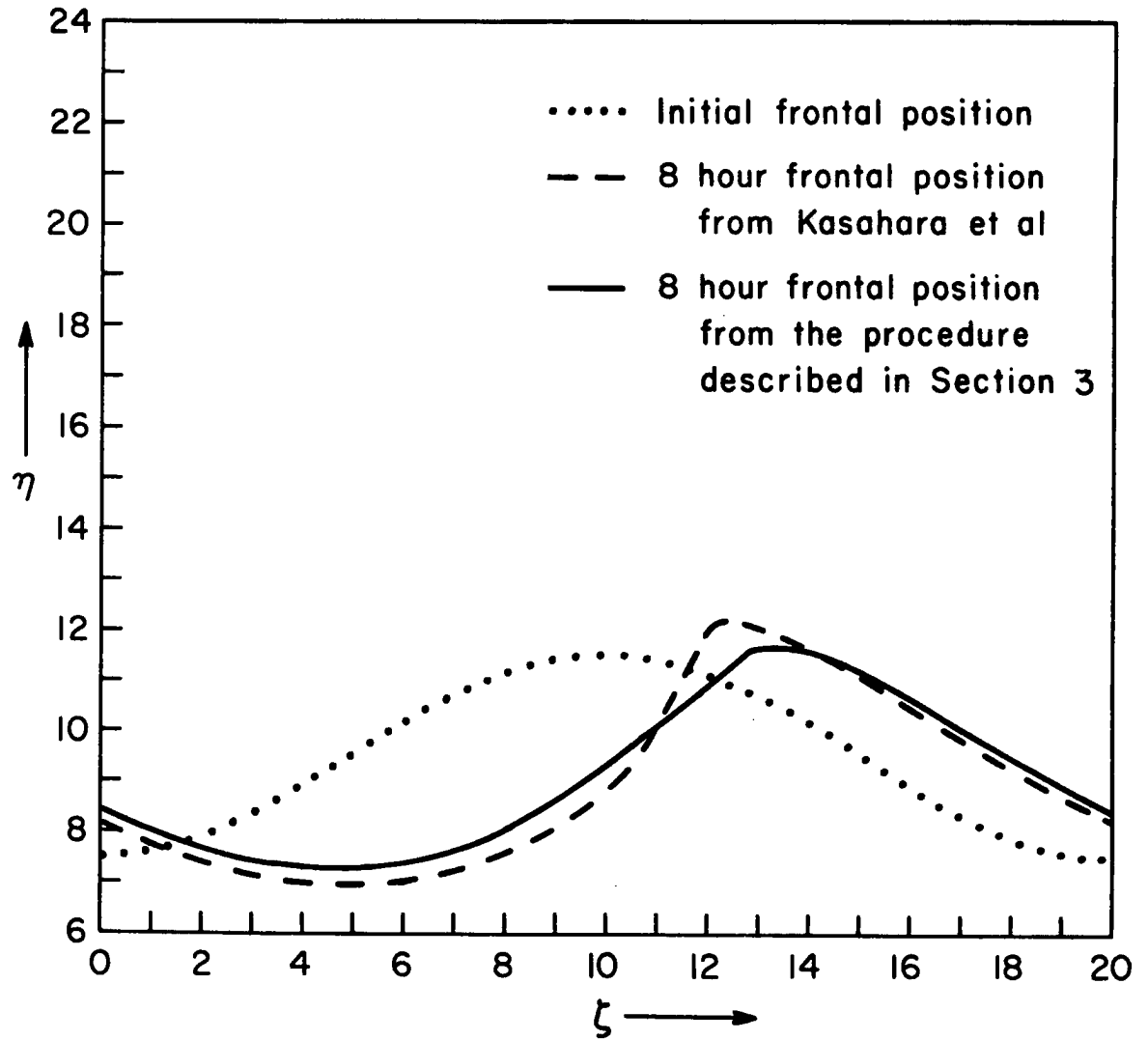


Figure 4

Initial and eight hour frontal positions calculated from "one layer" models.

same initial conditions used in the one layer case, the frontal motion was determined for a system which included an upper layer having a depth of 18 km at the southern boundary. A time sequence of frontal positions was constructed for both the one layer case (Figure 5) and the two layer case (Figure 6). Wind direction and velocity in the cold air is shown for the ninth hour. The unusual kinematic structures in the one layer case (Figure 5 points A and B) apparently result from the inability of the cold layer to adequately adjust its mass in response to the dynamics. This is a direct result of the neglect of the warm layer perturbations. The most unrealistic feature of the one layer calculation is the direction of flow of the cold air around the crest of the wave. This flow cannot easily be reconciled in terms of the characteristic circulation associated with developing frontal waves. In contrast, the two layer model appears to be in good agreement with the observed kinematics for a developing wave. Counter clockwise flow has developed around the wave and warm frontogenesis has appeared at the ninth hour.

In order to explain the southward shift of the entire front in the initial stages of integration (Figure 6, sixth hour), a more detailed analysis was performed on the first six hours of frontal motion. The analysis indicated that several hours were required for the initial wind and height fields to adjust to the unbalanced initial conditions. At time  $t = 0$ , the zonal wind was in geostrophic balance while the meridional wind was left unbalanced and set equal to zero (refer to initial condition, Table 1, column A). In response to this imbalance, the cold air rapidly accelerated southward. The one layer case required about four hours to

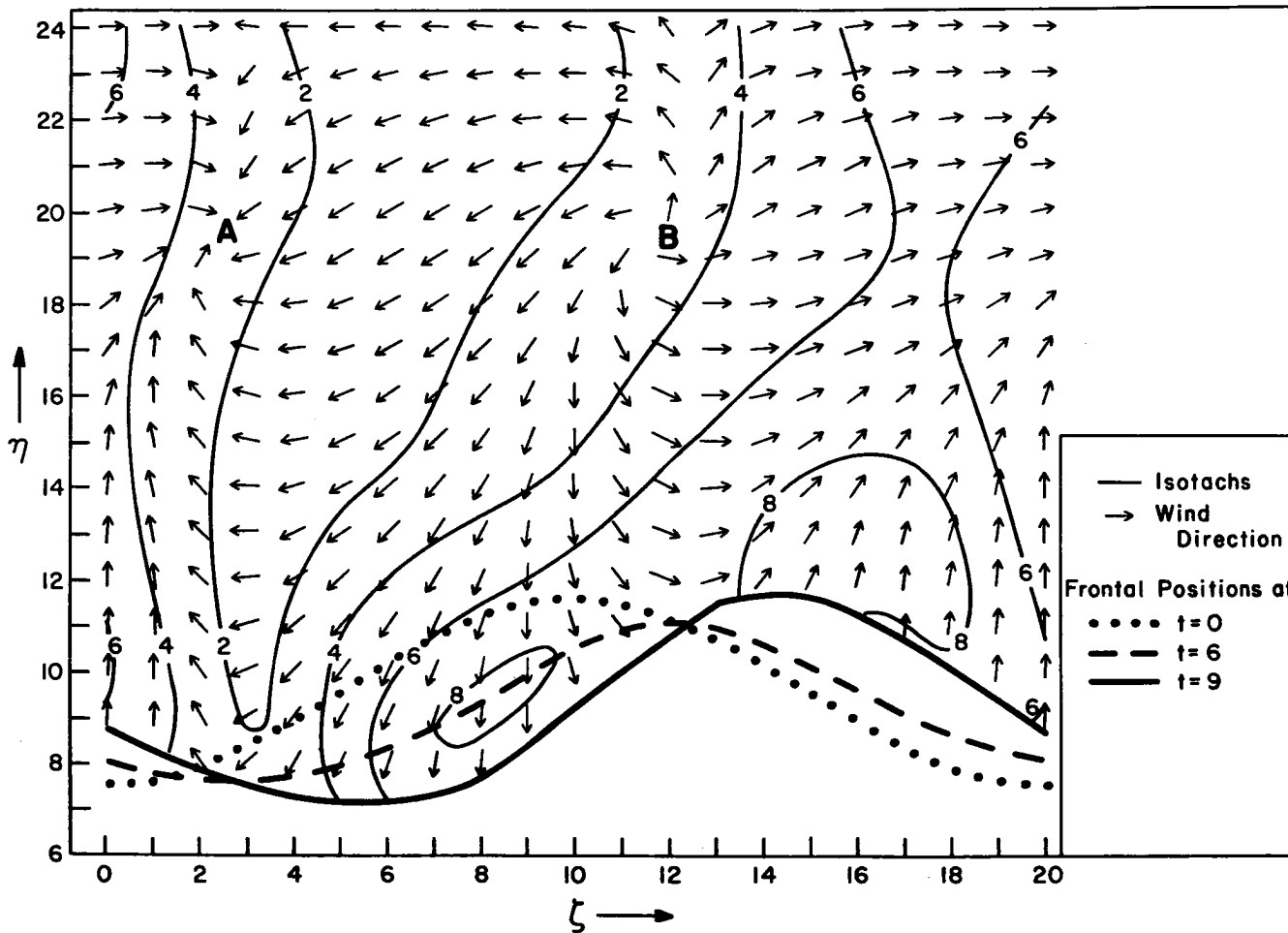


Figure 5  
 Frontal movement and ninth hour wind speed and direction for the "one layer" model.  
 Wind speed is given in meters per second.

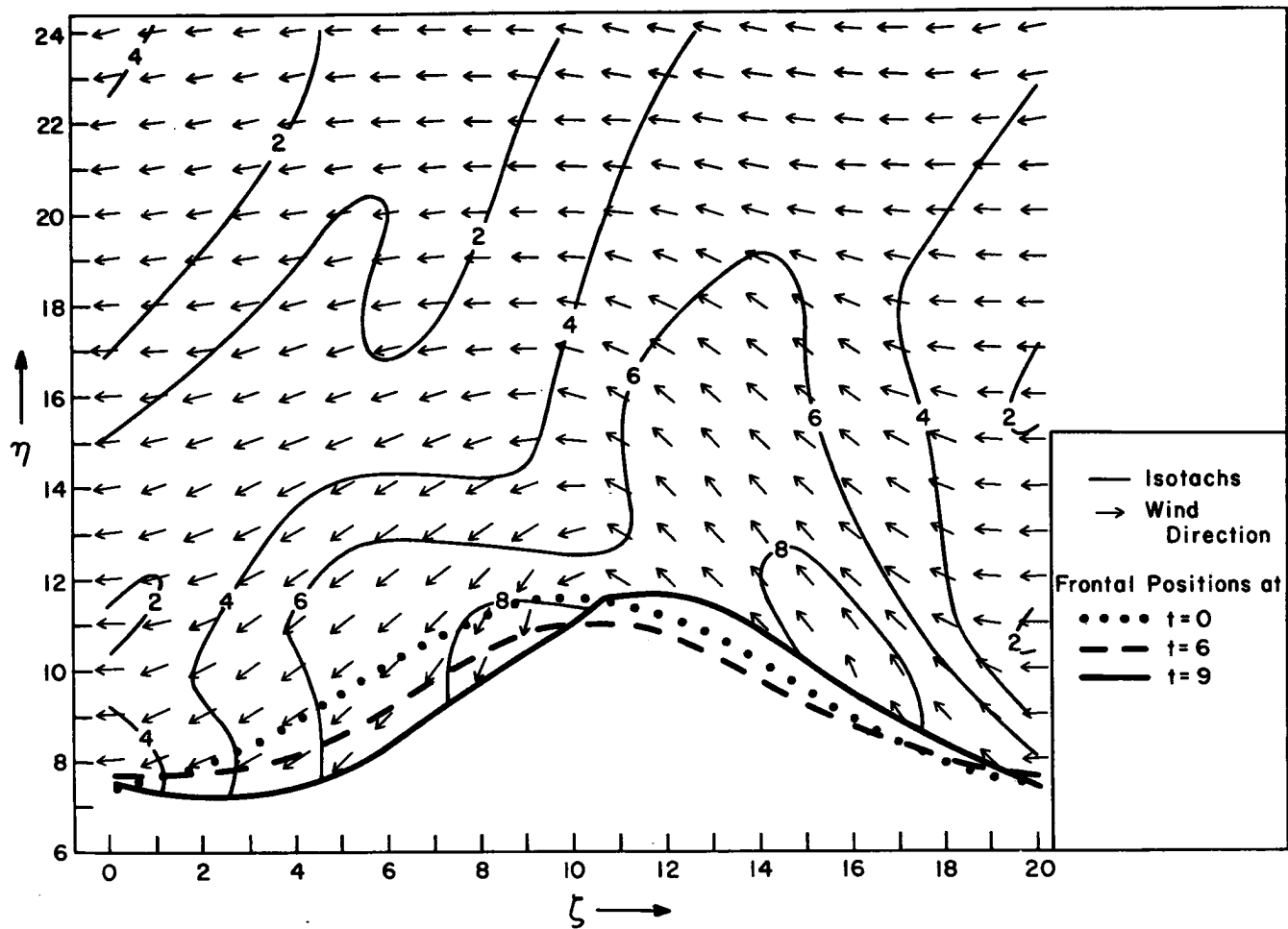


Figure 6

Frontal movement and ninth hour wind speed and direction for the two layer model.

Wind speed is given in meters per second.

correct the imbalance while the two layer case needed approximately five. This rapid "sinking" of cold air was accompanied by a corresponding increase in kinetic energy. Figure 7 shows the change in total kinetic energy (relative to the moving coordinate system) during the adjustment periods. During this process the change in total energy, kinetic plus potential, was less than a tenth of a percent in the eight hour period for both cases.

In addition to the effects discussed above, the inclusion of the upper layer dynamics reduced the wave speed from approximately 17 meters per second in the one layer case to about 10 meters per second in the two layer case. Thus it seems that the general effect of including the warm air perturbations is an overall stabilization of the system.

Following the investigation into the effects of imposing an upper layer on the frontal system, an effort was made to study the individual effects on the frontal motion due to specific parameters. In order to make such a study, a mean or basic set of initial conditions, representative of frequently observed atmospheric conditions, was defined. Once the behavior of the front was determined for these mean conditions, a single parameter such as shear or wavelength could be varied and its effects isolated. As discussed previously, the use of the geostrophic balance only in the zonal wind field required a significant amount of time to set up a reasonable kinematic structure. Therefore, it was decided to begin integration with the cold layer in total geostrophic balance. The complete set of base conditions is shown in Table 1, column B. Previous results, for example the warm frontogenesis at the ninth hour of the two layer model (Figure 6), indicated that perhaps

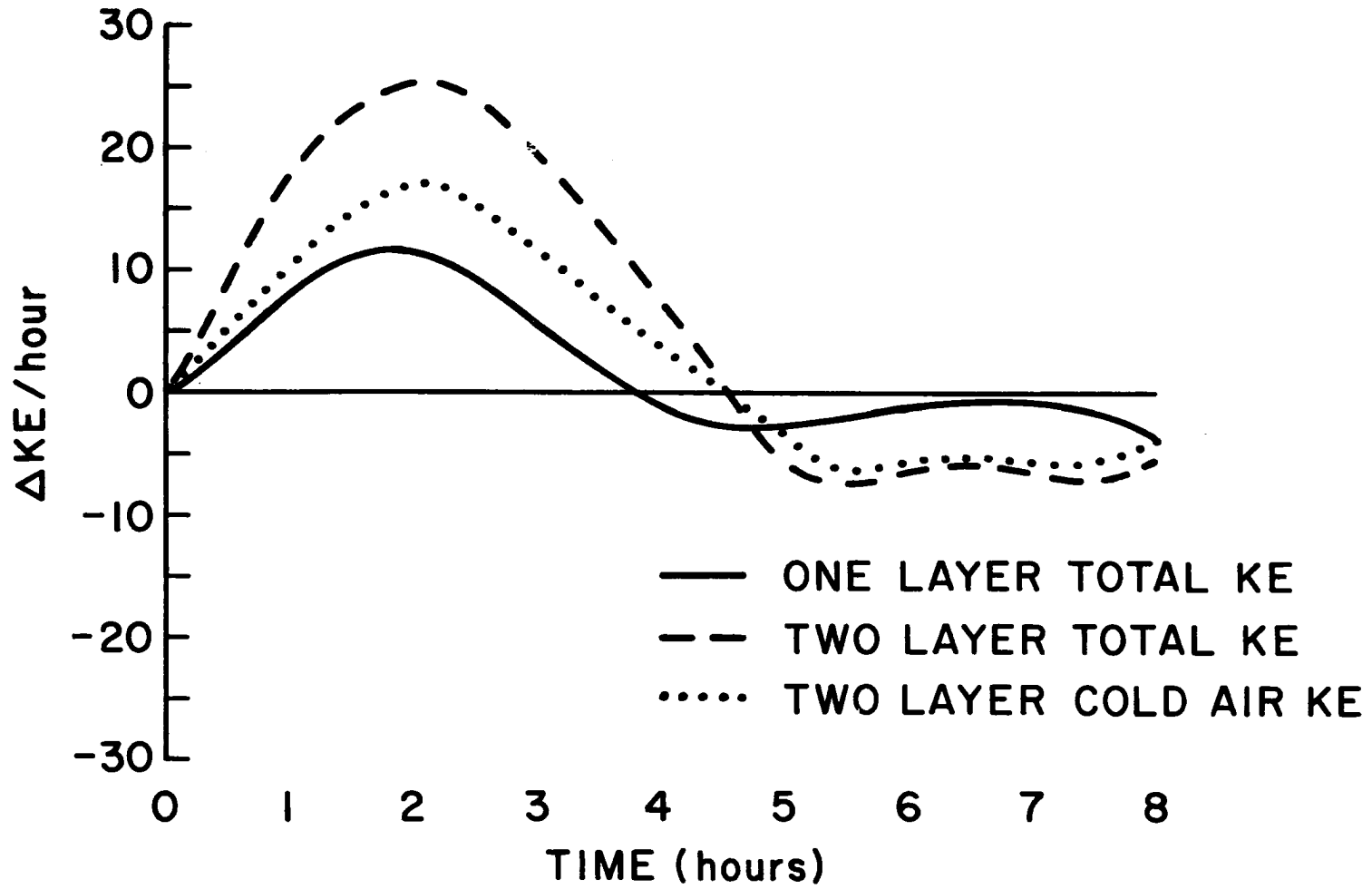


Figure 7

Change in total kinetic energy with time.

additional time was required for instability to develop. This seemed particularly true since the upper layer acted as a stabilizing force on the entire system. Thus, the geostrophic base state was integrated for 36 hours real time. The results are shown in Figure 8. In general, the base condition produced a slow moving, slightly decaying, easterly propagating wave.

Having generated the reference case, the following two special cases were investigated: 1) wavelength increased to one and one-half times the base wavelength; and 2) shear increased to twice the base shear. After twelve hours, the long wavelength case produced no significant change from the base state results and was therefore terminated. The high shear case proved to be unstable and will be discussed in detail. Figure 9 shows the time sequence of development of the high shear case along with the wind speed and direction at the twelfth hour. All analyses shown are relative to the moving coordinate system. Although the positions of the model's wind speed maxima and minima generally agree with observed positions, the magnitude of the wind speed maxima (24 and 12 meters per second) are rather large for surface winds (normally 5 to 10 meters per second). Considering that the model is friction-less and that the wind speed is indicative of the mean speed for the layer, perhaps 850 or 700 mb wind speeds would be more suitable for comparison. In this case the wind speeds are reasonable. Figures 10 and 11 show the wind direction and vorticity patterns at the twelfth hour for both the upper and lower layers. The initially zonal warm layer has interacted with the cold layer to produce an upper level trough to the west of the low level trough, which agrees with baroclinic theory. Considerable vorticity advection and associated divergence developed in advance of the upper

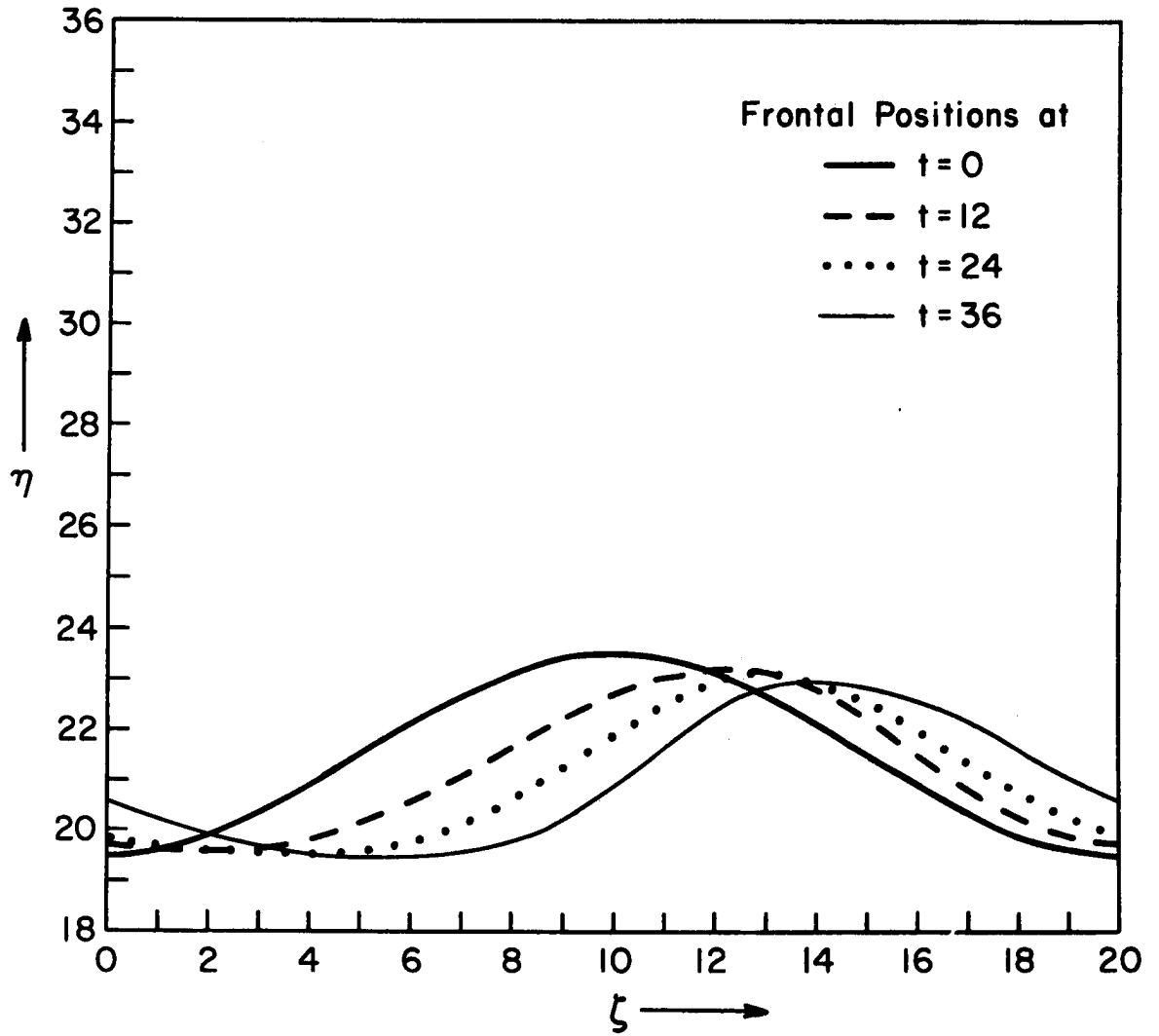


Figure 8  
Frontal movement during thirty-six hour integration  
of base-state two-layer model.

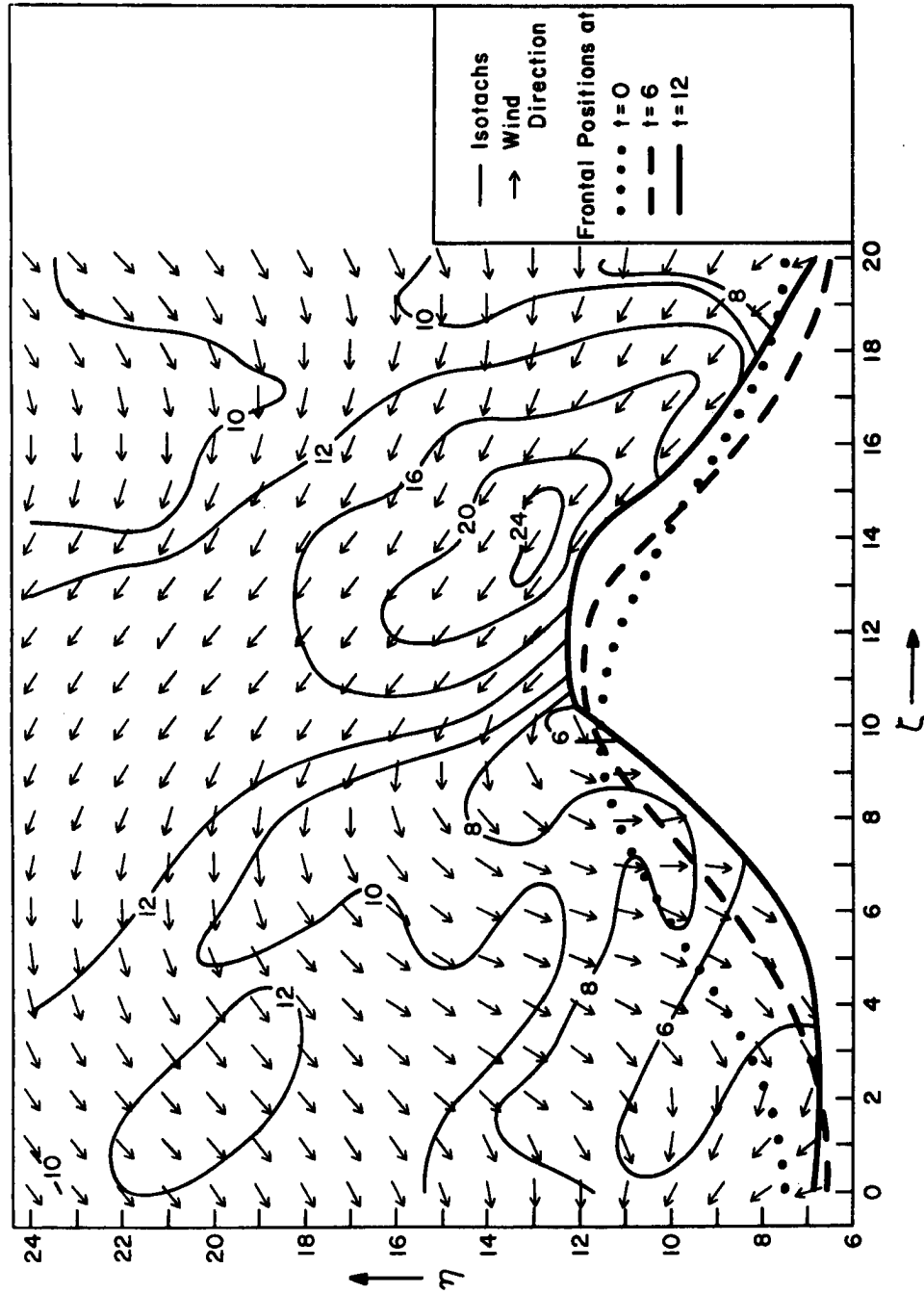


Figure 9

Frontal movement and twelfth hour wind speed and direction for the high shear case of the two layer model. Wind speed is in meters per second.

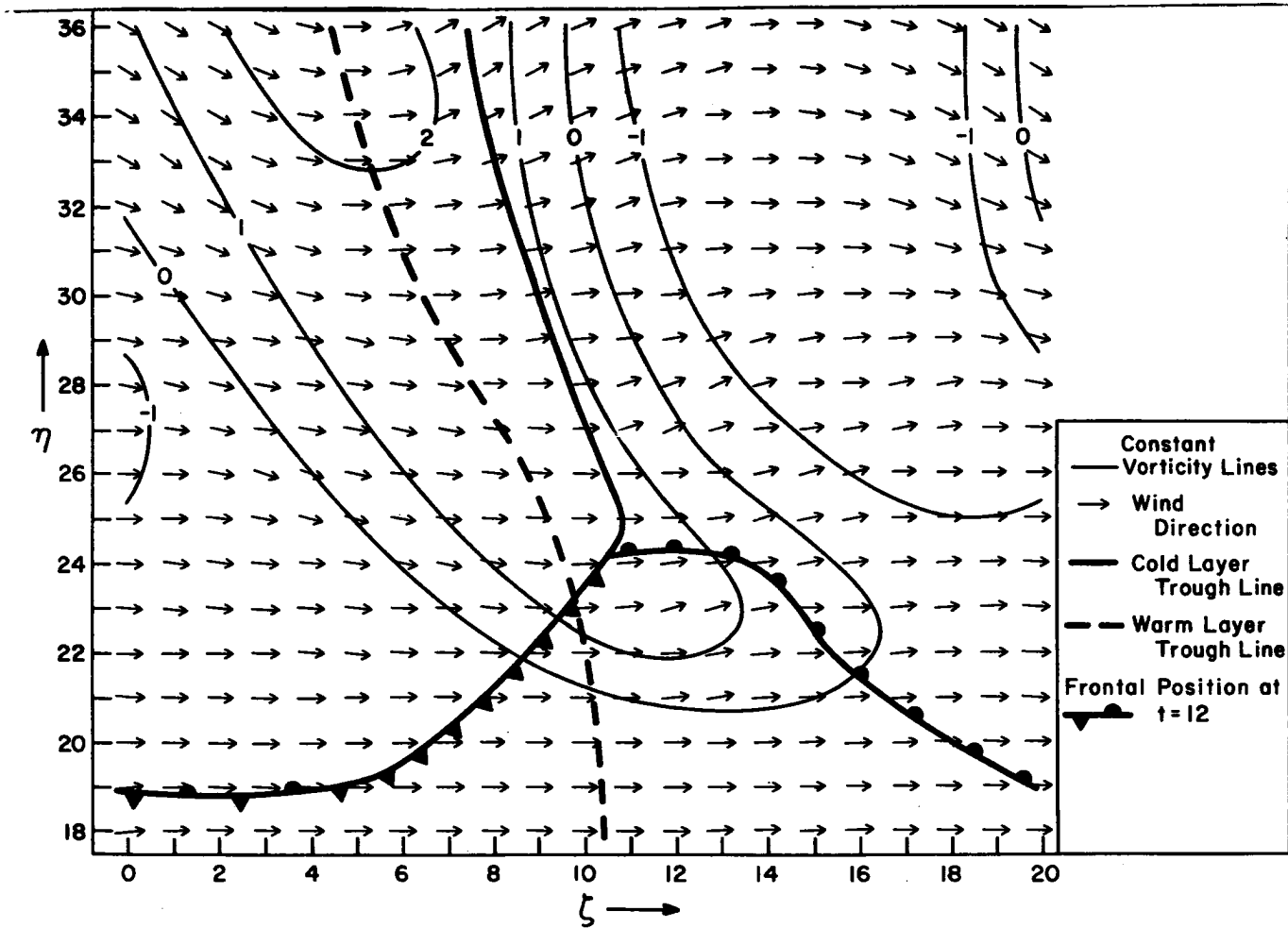


Figure 10

Twelfth hour wind direction, vorticity, and trough line in the warm layer.

Lines of constant vorticity are shown in non-dimensional units where 3.0 (non-dimensional) corresponds to  $5.0 \times 10^{-5} \text{ sec}^{-1}$ .

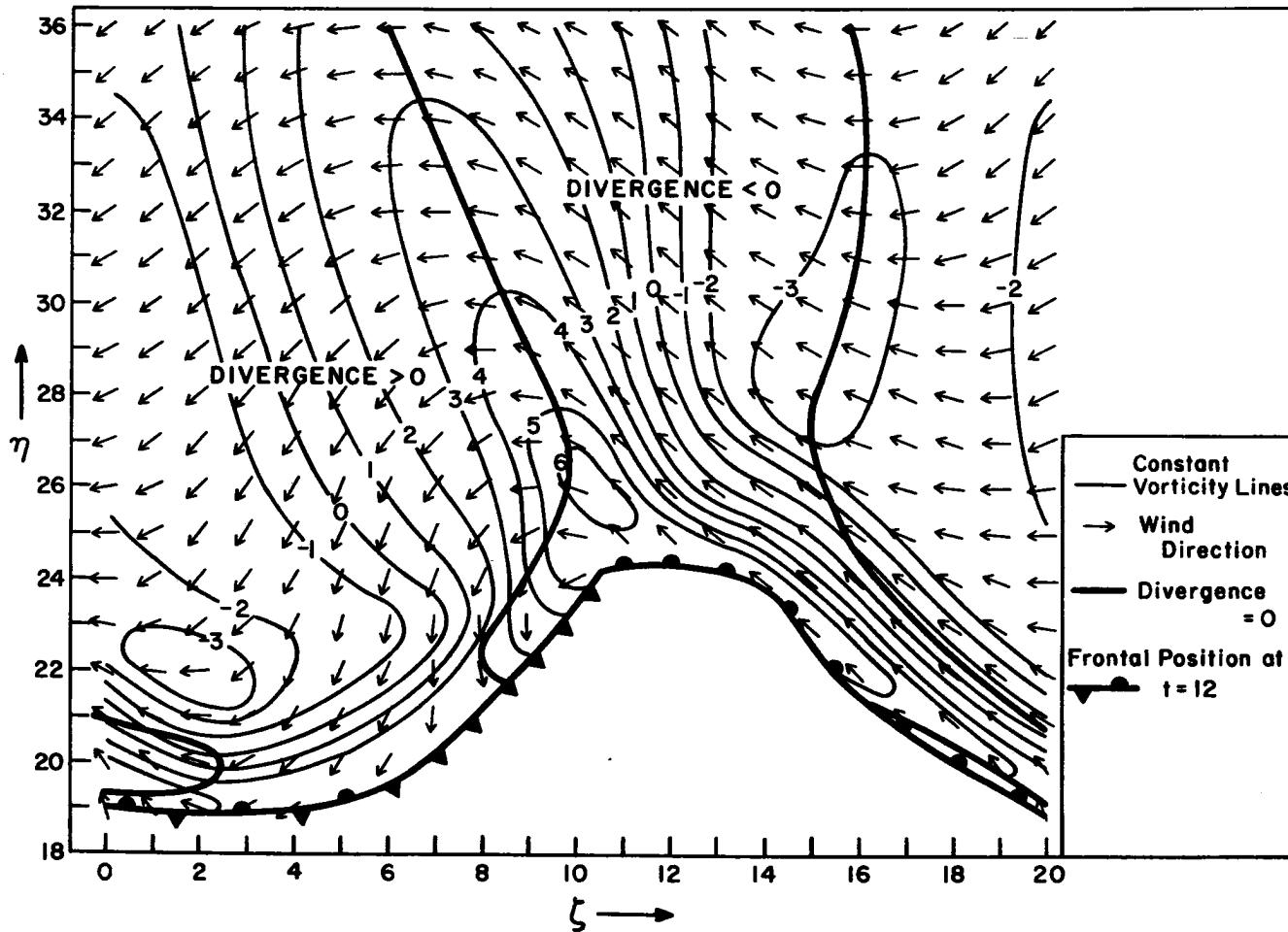


Figure 11

Twelfth hour wind direction, vorticity, and divergence in the cold layer. Lines of constant vorticity are shown in non dimensional units where 3.0 (non-dimensional) corresponds to  $5.0 \times 10^{-5} \text{ sec}^{-1}$ .

trough. As would be expected, convergence developed ahead of the trough in the cold layer. Similarly, upper level convergence and low level divergence developed behind the trough.

Relative to the ground, the speed of both the cold and warm fronts was slightly faster than normal. The average speed of the cold front was about 14 meters per second while the warm front moved at about 12 meters per second. Due to a numerical limitation on the technique used for calculating the frontal position, it was not possible to continue the integration past the point where the front ceased to be a single-valued function. Thus the frontal model could not be integrated to the occlusion stage. The relative speeds of the cold and warm fronts, however, suggest that occlusion would occur.

## 5. CONCLUSION

The two layer frontal model appears to be capable of reproducing the basic features of developing frontal waves. Circulation around the model wave agrees with most observations and the corresponding fields of vorticity and divergence support the general baroclinic theory associated with developing cyclones. Although the limitations of the numerical scheme prevented integration of the frontal motion past occlusion, the results agreed rather well with observed frontal behavior and indicated an occlusion process would occur. The overall effect of including the dynamics of an upper layer seems to be a general stabilization of the entire system. Since the normal initial upper air streamflow pattern associated with developing waves is very rarely zonal, this stabilizing effect may be peculiar to our initial conditions. In the real atmosphere there is frequently a substantial degree of upper level support in the form of a cold core high level synoptic scale wave. Normally, this synoptic wave propagates eastward above the low level frontal system and interacts with it. The strength of the upper support is highly variable and depends, among other things, on the intensity and orientation of the upper wave with respect to the front. Thus, for the model's case, if the upper layer would have initially been in a position to support surface development, the potential energy consumed to deform the zonal upper layer could have been used for wave development.

Although the results of this study are indicative of the importance of the upper layer, in view of the above discussion, it seems logical that the next step in an attempt to understand the mechanism at work in frontal wave development would be to begin integration with a wave

in the upper level. However, from Grammelvedt (1970), it appears that the effect of introducing the initial disturbance either in the upper layer alone, or in both layers, is not likely to modify the results in any significant manner.

## References

- Abdullah, A. J., 1949: Cyclogenesis by a purely mechanical process.  
Jour. Met., 6, 86-97.
- Alterman, Z. S. and E. Isaacson, 1969: A method for calculating frontal motion - I. Journal Computational Physics.
- Bjerknes, J. and C. L. Godske, 1936: On the theory of cyclone formation at extra-tropical fronts. Astrophysica Norvegica, 1, 199-235.
- Bjerknes, J. and H. Solberg, 1922: Life cycle of cyclones and polar front theory of atmospheric circulation. Geofysiske Publikasjoner, 3, No. 1.
- Eliassen, E., 1960: On the initial development of frontal waves.  
Publikationer fra Det Danske Meteorologiske Institut, No. 13,  
107 pp.
- Eliassen, A. and Elmer Ranstein, 1968: A numerical integration experiment with a model atmosphere based on isentropic surfaces. Meteorologiske Annaler, 5, 45-63.
- Freeman, J. C., Jr., 1952: Flow under an inversion in middle latitudes.  
Ph.D. Dissertation. University of Chicago, 59 pp.
- Grammeltvedt, A., 1970: Numerical simulation of the motion of atmospheric fronts using a two layer model. Tellus, 22, 627-637.
- Kasahara, A., E. Isaacson and J. J. Stoker, 1965: Numerical studies of frontal motion in the atmosphere - I. Tellus, 17, 261-276.
- Kotschin, N., 1932: Über die stabilität von Marguelesschen Diskontinuitätsflächen. Beiträge zur der freien Atmosphäre, 18, 129-164.
- Lilly, D. K., 1965: On the computational stability of numerical solutions of time-dependent non-linear geophysical fluid dynamics problems.  
Monthly Weather Review, 93, 11-26.

Unclassified

Security Classification

14.	KEY WORDS	LINK A		LINK B		LINK C	
		ROLE	WT	ROLE	WT	ROLE	WT
	Numerical frontal model Frontal wave development						

Unclassified

Security Classification